

DESY 01–062
May 2001

ISSN 0418–9833

Photoproduction with a Leading Proton at HERA

H1 Collaboration

Abstract

The total cross section for the photoproduction process with a leading proton in the final state has been measured at γp centre-of-mass energies W of 91, 181 and 231 GeV. The measured cross sections apply to the kinematic range with the transverse momentum of the scattered proton restricted to $p_T \leq 0.2$ GeV and $0.68 \leq z \leq 0.88$, where $z = E'_p/E_p$ is the scattered proton energy normalised to the beam energy. The cross section $d\sigma_{\gamma p \rightarrow X p'}(W, z)/dz$ is observed to be independent of W and z within the measurement errors and amounts to $(8.05 \pm 0.06 \text{ (stat)} \pm 0.89 \text{ (syst)}) \mu\text{b}$ on average. The data are well described by a Triple Regge model in which the process is mediated by a mixture of exchanges with an effective Regge trajectory of intercept $\alpha_i(0) = 0.33 \pm 0.04 \text{ (stat)} \pm 0.04 \text{ (syst)}$. The total cross section for the interaction of the photon with this mixture ($\gamma \alpha_i \rightarrow X$) can be described by an effective trajectory of intercept $\alpha_k(0) = 0.99 \pm 0.01 \text{ (stat)} \pm 0.05 \text{ (syst)}$. Predictions based on previous triple Regge analyses of $pp \rightarrow pX$ data assuming vertex factorisation are broadly consistent with the γp data. The measured cross sections are compared with deep inelastic scattering leading proton data in the same region of z and p_T for photon virtuality $Q^2 > 2.5$ GeV 2 . The ratio of the cross section for leading proton production to the total cross section is found to rise with Q^2 .

To be submitted to *Nucl. Phys. B*

C. Adloff³³, V. Andreev²⁴, B. Andrieu²⁷, T. Anthonis⁴, V. Arkadov³⁵, A. Astvatsatourov³⁵, I. Ayyaz²⁸, A. Babaev²³, J. Bähr³⁵, P. Baranov²⁴, E. Barrelet²⁸, W. Bartel¹⁰, P. Bate²¹, A. Beglarian³⁴, O. Behnke¹³, C. Beier¹⁴, A. Belousov²⁴, T. Benisch¹⁰, Ch. Berger¹, T. Berndt¹⁴, J.C. Bizot²⁶, V. Boudry²⁷, W. Braunschweig¹, V. Brisson²⁶, H.-B. Bröker², D.P. Brown¹¹, W. Brückner¹², P. Bruel²⁷, D. Bruncko¹⁶, J. Bürger¹⁰, F.W. Büsser¹¹, A. Bunyatyan^{12,34}, H. Burkhardt¹⁴, A. Burrage¹⁸, G. Buschhorn²⁵, A.J. Campbell¹⁰, J. Cao²⁶, T. Carli²⁵, S. Caron¹, E. Chabert²², D. Clarke⁵, B. Clerbaux⁴, C. Collard⁴, J.G. Contreras^{7,41}, Y.R. Coppens³, J.A. Coughlan⁵, M.-C. Cousinou²², B.E. Cox²¹, G. Cozzika⁹, J. Cvach²⁹, J.B. Dainton¹⁸, W.D. Dau¹⁵, K. Daum^{33,39}, M. Davidsson²⁰, B. Delcourt²⁶, N. Delerue²², R. Demirchyan³⁴, A. De Roeck^{10,43}, E.A. De Wolf⁴, C. Diaconu²², P. Dixon¹⁹, V. Dodonov¹², J.D. Dowell³, A. Droutskoi²³, C. Duprel², G. Eckerlin¹⁰, D. Eckstein³⁵, V. Efremenko²³, S. Egli³², R. Eichler³⁶, F. Eisele¹³, E. Eisenhandler¹⁹, M. Ellerbrock¹³, E. Elsen¹⁰, M. Erdmann^{10,40,e}, W. Erdmann³⁶, P.J.W. Faulkner³, L. Favart⁴, A. Fedotov²³, R. Felst¹⁰, J. Ferencei¹⁰, S. Ferron²⁷, M. Fleischer¹⁰, Y.H. Fleming³, G. Flügge², A. Fomenko²⁴, I. Foresti³⁷, J. Formánek³⁰, J.M. Foster²¹, G. Franke¹⁰, E. Gabathuler¹⁸, K. Gabathuler³², J. Garvey³, J. Gassner³², J. Gayler¹⁰, R. Gerhards¹⁰, S. Ghazaryan³⁴, L. Goerlich⁶, N. Gogitidze²⁴, M. Goldberg²⁸, C. Goodwin³, C. Grab³⁶, H. Grässler², T. Greenshaw¹⁸, G. Grindhammer²⁵, T. Hadig¹³, D. Haidt¹⁰, L. Hajduk⁶, W.J. Haynes⁵, B. Heinemann¹⁸, G. Heinzelmann¹¹, R.C.W. Henderson¹⁷, S. Hengstmann³⁷, H. Henschel³⁵, R. Heremans⁴, G. Herrera^{7,41}, I. Herynek²⁹, M. Hildebrandt³⁷, M. Hilgers³⁶, K.H. Hiller³⁵, J. Hladký²⁹, P. Höting², D. Hoffmann¹⁰, R. Horisberger³², S. Hurling¹⁰, M. Ibbotson²¹, Ç. İşsever⁷, M. Jacquet²⁶, M. Jaffre²⁶, L. Janauschek²⁵, D.M. Jansen¹², X. Janssen⁴, V. Jemanov¹¹, L. Jönsson²⁰, D.P. Johnson⁴, M.A.S. Jones¹⁸, H. Jung¹⁰, H.K. Kästli³⁶, D. Kant¹⁹, M. Kapichine⁸, M. Karlsson²⁰, O. Karschnick¹¹, F. Keil¹⁴, N. Keller³⁷, J. Kennedy¹⁸, I.R. Kenyon³, S. Kermiche²², C. Kiesling²⁵, P. Kjellberg²⁰, M. Klein³⁵, C. Kleinwort¹⁰, G. Knies¹⁰, B. Koblitz²⁵, S.D. Kolya²¹, V. Korbel¹⁰, P. Kostka³⁵, S.K. Kotelnikov²⁴, R. Koutouev¹², A. Koutov⁸, M.W. Krasny²⁸, H. Krehbiel¹⁰, J. Kroeseberg³⁷, K. Krüger¹⁰, A. Küpper³³, T. Kuhr¹¹, T. Kurča^{35,16}, R. Lahmann¹⁰, D. Lamb³, M.P.J. Landon¹⁹, W. Lange³⁵, T. Laštovička³⁰, P. Laycock¹⁸, E. Lebailly²⁶, A. Lebedev²⁴, B. Leißner¹, R. Lemrani¹⁰, V. Lendermann⁷, S. Levonian¹⁰, M. Lindstroem²⁰, B. List³⁶, E. Lobodzinska^{10,6}, B. Lobodzinski^{6,10}, A. Loginov²³, N. Loktionova²⁴, V. Lubimov²³, S. Lüders³⁶, D. Lüke^{7,10}, L. Lytkin¹², N. Magnussen³³, H. Mahlke-Krüger¹⁰, N. Malden²¹, E. Malinovski²⁴, I. Malinovski²⁴, R. Maraček²⁵, P. Marage⁴, J. Marks¹³, R. Marshall²¹, H.-U. Martyn¹, J. Martyniak⁶, S.J. Maxfield¹⁸, A. Mehta¹⁸, K. Meier¹⁴, P. Merkel¹⁰, A.B. Meyer¹¹, H. Meyer³³, J. Meyer¹⁰, P.-O. Meyer², S. Mikocki⁶, D. Milstead¹⁸, T. Mkrtchyan³⁴, R. Mohr²⁵, S. Mohrdieck¹¹, M.N. Mondragon⁷, F. Moreau²⁷, A. Morozov⁸, J.V. Morris⁵, K. Müller¹³, P. Murín^{16,42}, V. Nagovizin²³, B. Naroska¹¹, J. Naumann⁷, Th. Naumann³⁵, G. Nellen²⁵, P.R. Newman³, T.C. Nicholls⁵, F. Niebergall¹¹, C. Niebuhr¹⁰, O. Nix¹⁴, G. Nowak⁶, T. Nunnemann¹², J.E. Olsson¹⁰, D. Ozerov²³, V. Panassik⁸, C. Pascaud²⁶, G.D. Patel¹⁸, E. Perez⁹, J.P. Phillips¹⁸, D. Pitzl¹⁰, R. Pöschl⁷, I. Potachnikova¹², B. Povh¹², K. Rabbertz¹, G. Rädel¹, J. Rauschenberger¹¹, P. Reimer²⁹, B. Reisert²⁵, D. Reyna¹⁰, S. Riess¹¹, C. Risler²⁵, E. Rizvi³, P. Robmann³⁷, R. Roosen⁴, A. Rostovtsev²³, C. Royon⁹, S. Rusakov²⁴, K. Rybicki⁶, D.P.C. Sankey⁵, J. Scheins¹, F.-P. Schilling¹³, P. Schleper¹⁰, D. Schmidt³³, D. Schmidt¹⁰, S. Schmitt¹⁰, L. Schoeffel⁹, A. Schöning³⁶, T. Schörner²⁵, V. Schröder¹⁰, H.-C. Schultz-Coulon⁷, C. Schwanenberger¹⁰, K. Sedláček²⁹, F. Sefkow³⁷, V. Shekelyan²⁵, I. Sheviakov²⁴, L.N. Shtarkov²⁴, P. Sievers¹³, Y. Sirois²⁷, T. Sloan¹⁷, P. Smirnov²⁴,

V. Solochenko^{23,†}, Y. Soloviev²⁴, V. Spaskov⁸, A. Specka²⁷, H. Spitzer¹¹, R. Stamen⁷,
 J. Steinhart¹¹, B. Stella³¹, A. Stellberger¹⁴, J. Stiewe¹⁴, U. Straumann³⁷, W. Struczinski²,
 M. Swart¹⁴, M. Taševský²⁹, V. Tchernyshov²³, S. Tchetchelnitski²³, G. Thompson¹⁹,
 P.D. Thompson³, N. Tobien¹⁰, D. Traynor¹⁹, P. Truöl³⁷, G. Tsipolitis^{10,38}, I. Tsurin³⁵,
 J. Turnau⁶, J.E. Turney¹⁹, E. Tzamariudaki²⁵, S. Udluft²⁵, A. Usik²⁴, S. Valkár³⁰,
 A. Valkárová³⁰, C. Vallée²², P. Van Mechelen⁴, S. Vassiliev⁸, Y. Vazdik²⁴, A. Vichnevski⁸,
 K. Wacker⁷, R. Wallny³⁷, T. Walter³⁷, B. Waugh²¹, G. Weber¹¹, M. Weber¹⁴, D. Wegener⁷,
 M. Werner¹³, G. White¹⁷, S. Wiesand³³, T. Wilksen¹⁰, M. Winde³⁵, G.-G. Winter¹⁰,
 Ch. Wissing⁷, M. Wobisch², H. Wollatz¹⁰, E. Wünsch¹⁰, A.C. Wyatt²¹, J. Žáček³⁰,
 J. Zálešák³⁰, Z. Zhang²⁶, A. Zhokin²³, F. Zomer²⁶, J. Zsembery⁹, and M. zur Nedden¹⁰

¹ *I. Physikalisches Institut der RWTH, Aachen, Germany^a*

² *III. Physikalisches Institut der RWTH, Aachen, Germany^a*

³ *School of Physics and Space Research, University of Birmingham, Birmingham, UK^b*

⁴ *Inter-University Institute for High Energies ULB-VUB, Brussels; Universitaire Instelling Antwerpen, Wilrijk; Belgium^c*

⁵ *Rutherford Appleton Laboratory, Chilton, Didcot, UK^b*

⁶ *Institute for Nuclear Physics, Cracow, Poland^d*

⁷ *Institut für Physik, Universität Dortmund, Dortmund, Germany^a*

⁸ *Joint Institute for Nuclear Research, Dubna, Russia*

⁹ *CEA, DSM/DAPNIA, CE-Saclay, Gif-sur-Yvette, France*

¹⁰ *DESY, Hamburg, Germany^a*

¹¹ *II. Institut für Experimentalphysik, Universität Hamburg, Hamburg, Germany^a*

¹² *Max-Planck-Institut für Kernphysik, Heidelberg, Germany^a*

¹³ *Physikalisches Institut, Universität Heidelberg, Heidelberg, Germany^a*

¹⁴ *Kirchhoff-Institut für Physik, Universität Heidelberg, Heidelberg, Germany^a*

¹⁵ *Institut für experimentelle und angewandte Kernphysik, Universität Kiel, Kiel, Germany^a*

¹⁶ *Institute of Experimental Physics, Slovak Academy of Sciences, Košice, Slovak Republic^{e,f}*

¹⁷ *School of Physics and Chemistry, University of Lancaster, Lancaster, UK^b*

¹⁸ *Department of Physics, University of Liverpool, Liverpool, UK^b*

¹⁹ *Queen Mary and Westfield College, London, UK^b*

²⁰ *Physics Department, University of Lund, Lund, Sweden^g*

²¹ *Physics Department, University of Manchester, Manchester, UK^b*

²² *CPPM, CNRS/IN2P3 - Univ Méditerranée, Marseille - France*

²³ *Institute for Theoretical and Experimental Physics, Moscow, Russia*

²⁴ *Lebedev Physical Institute, Moscow, Russia^{e,h}*

²⁵ *Max-Planck-Institut für Physik, München, Germany^a*

²⁶ *LAL, Université de Paris-Sud, IN2P3-CNRS, Orsay, France*

²⁷ *LPNHE, Ecole Polytechnique, IN2P3-CNRS, Palaiseau, France*

²⁸ *LPNHE, Universités Paris VI and VII, IN2P3-CNRS, Paris, France*

²⁹ *Institute of Physics, Czech Academy of Sciences, Praha, Czech Republic^{e,i}*

³⁰ *Faculty of Mathematics and Physics, Charles University, Praha, Czech Republic^{e,i}*

³¹ *Dipartimento di Fisica Università di Roma Tre and INFN Roma 3, Roma, Italy*

³² *Paul Scherrer Institut, Villigen, Switzerland*

³³ *Fachbereich Physik, Bergische Universität Gesamthochschule Wuppertal, Wuppertal, Germany^a*

³⁴ *Yerevan Physics Institute, Yerevan, Armenia*

³⁵ *DESY, Zeuthen, Germany^a*

³⁶ *Institut für Teilchenphysik, ETH, Zürich, Switzerland^j*

³⁷ *Physik-Institut der Universität Zürich, Zürich, Switzerland^j*

³⁸ *Also at Physics Department, National Technical University, Zografou Campus, GR-15773 Athens, Greece*

³⁹ *Also at Rechenzentrum, Bergische Universität Gesamthochschule Wuppertal, Germany*

⁴⁰ *Also at Institut für Experimentelle Kernphysik, Universität Karlsruhe, Karlsruhe, Germany*

⁴¹ *Also at Dept. Fis. Ap. CINVESTAV, Mérida, Yucatán, México^k*

⁴² *Also at University of P.J. Šafárik, Košice, Slovak Republic*

⁴³ *Also at CERN, Geneva, Switzerland*

† *Deceased*

^a *Supported by the Bundesministerium für Bildung, Wissenschaft, Forschung und Technologie, FRG, under contract numbers 7AC17P, 7AC47P, 7DO55P, 7HH17I, 7HH27P, 7HD17P, 7HD27P, 7KI17I, 6MP17I and 7WT87P*

^b *Supported by the UK Particle Physics and Astronomy Research Council, and formerly by the UK Science and Engineering Research Council*

^c *Supported by FNRS-NFWO, IISN-IIKW*

^d *Partially Supported by the Polish State Committee for Scientific Research, grant no.*

2P0310318 and SPUB/DESY/P03/DZ-1/99, and by the German Federal Ministry of Education and Science, Research and Technology (BMBF)

^e *Supported by the Deutsche Forschungsgemeinschaft*

^f *Supported by VEGA SR grant no. 2/5167/98*

^g *Supported by the Swedish Natural Science Research Council*

^h *Supported by Russian Foundation for Basic Research grant no. 96-02-00019*

ⁱ *Supported by GA AV ČR grant no. A1010821*

^j *Supported by the Swiss National Science Foundation*

^k *Supported by CONACyT*

1 Introduction

Over the years there has been considerable interest in “diffractive” dissociation processes in strong interactions. At pp collider experiments, the reaction $pp \rightarrow Xp'$ has been studied in detail [1, 2], whilst at HERA the process $\gamma p \rightarrow Xp'$ has also been closely investigated for both real and virtual photons [3–8]. These processes are often interpreted using Regge phenomenology in terms of the exchange of colourless objects between the colliding particles. Such scattering is distinguished in collider experiments by the observation of rapidity gaps between the beam direction and the produced hadrons, X . A complementary way to study these processes is by direct detection of the leading protons from the reactions.

At HERA, the nature of the exchange has been found to depend on the fraction of the beam longitudinal momentum retained by the final state proton, z ¹. When $z \rightarrow 1$, the cross section is well described by pomeron (\mathcal{P}) exchange in both photoproduction [4, 5] and Deep Inelastic Scattering (DIS) [6, 7]. At $z \sim 0.95$, additional meson trajectories associated with ρ , ω , f_2 or a_2 , here collectively denoted \mathcal{R} , have been found to contribute [4, 6]. In a previous publication [3] DIS data with a leading proton in the kinematic range $0.73 \leq z \leq 0.88$ were shown to be well described by a Regge model in which the virtual photon interacts with a mixture of exchanges dominated by \mathcal{R} and π . In this paper, we present measurements using the H1 Forward Proton Spectrometer (FPS) to reconstruct the proton momentum directly in a similar region of z to [3], but in the photoproduction limit. These measurements extend those of [4] to lower values of z .

The semi-inclusive scattering reaction $ep \rightarrow e'Xp'$ is sketched in figure 1. The measured process described in this paper is $\gamma p \rightarrow Xp'$ for quasi-real photons, in which the photon emitted by the incoming electron reacts with the proton to produce a system of mass M_X . The squared four-momentum transfer at the proton vertex is denoted by t . The proton remains intact leaving the interaction with an energy fraction $z = E'_p/E_p$, E'_p and E_p being the energies of the outgoing and incoming protons, respectively. For the elastic process shown in figure 1, the mass M_X is equal to $W\sqrt{1-z}$, where W is the centre-of-mass energy of the photon-proton system. In a Regge interpretation, the reaction proceeds via the exchange of an object \mathcal{R} .

The W and z dependences of the data are used to investigate the contributions of different exchanges away from the pomeron dominated region. Comparison is made with measurements of the process $pp \rightarrow Xp'$ using a model based on Regge phenomenology. Together with the data from DIS in [3] the photon virtuality, Q^2 , dependence of the semi-inclusive scattering process is investigated. This allows one to study how the dissociative process varies as the incoming particle changes from a point-like object at high Q^2 to a hadron-like object in the photoproduction region at $Q^2 = 0$. This transition has been studied in detail in inclusive scattering $ep \rightarrow e'X$ [9, 10], but no previous information exists for semi-inclusive processes at the values of z studied here.

2 Experimental Method

¹In some publications, $x_{pP} = 1 - z$ is used instead.

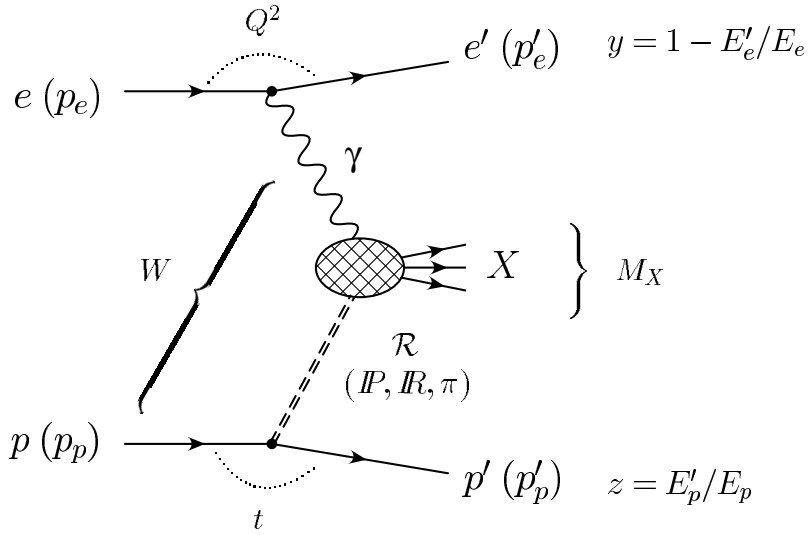


Figure 1: The leading proton process $ep \rightarrow e'p'X$ in a Regge exchange model. At the proton vertex, $z = E'_p/E_p$ is the energy fraction retained by the proton.

2.1 The H1 Detector

The H1 detector is described in detail elsewhere [11]. We use a coordinate system originating at the interaction point with the positive z axis along the proton beam direction. The selection of the final state of the reaction under study is performed by identifying the scattered proton, the scattered electron and at least one charged track in the central region of the H1 detector. The central tracking chambers and the central proportional chambers, located within the 1.15 Tesla field of the H1 solenoid, trigger on and measure the momentum of tracks, the resolution being $\Delta(p_t)/p_t^2 \sim 10^{-2} \text{ GeV}^{-1}$ for $p_t > 0.5 \text{ GeV}$. Small angle electron calorimeters and a photon detector are used to determine the luminosity via the Bethe-Heitler process $ep \rightarrow e'p'\gamma$, to tag photoproduction events and to suppress Bethe-Heitler background in the measurement. By selecting an electron candidate in the electron calorimeters, the acceptance is restricted to values of the photon virtuality $Q^2 < 0.01 \text{ GeV}^2$.

The Forward Proton Spectrometer (FPS) [3, 12] is used to measure the energy and scattering angles at the interaction point of the outgoing proton. Protons scattered at small angles to the incident proton direction are deflected by the magnets of the beam optics into a system of detectors placed close to the proton beam in moveable ‘‘Roman pot’’ housing stations, approaching the beam from above. The stations used in this analysis are positioned at distances of 81 and 90 m downstream of the interaction point and are moved into position once stable beam conditions are established. The pattern of hits from many events observed in the position detectors is analyzed to determine spatial offsets and tilts of the proton beam at the interaction point. For each event the outgoing proton energy and scattering angles are then obtained from the reconstructed track positions and the measured interaction point using the transfer functions derived from the beam optics [13]. The energy resolution deteriorates with energy and is better than 8 GeV. The absolute energy scale uncertainty is estimated to $\pm 10 \text{ GeV}$, as has been

inferred from a comparison of a diffractive model with the data and from a study of a small number of events at large Q^2 , where the kinematics are determined independently in the main detector [12, 13]. The mean error on the angle measurement is $5 \mu\text{rad}$ in the θ_x projection and varies with increasing beam energy from $5 \mu\text{rad}$ to $100 \mu\text{rad}$ in the θ_y projection. With a primary proton beam of 820 GeV , scattered proton energies in the range $500 \text{ GeV} < E'_p < 780 \text{ GeV}$ are accepted by the spectrometer. For a proton which passes through both stations, the average overall track reconstruction efficiency is approximately 50%.

2.2 Data Selection

The analysis is based on a data set from the 1996 running period, when HERA collided 820 GeV protons with 27.5 GeV positrons, resulting in an ep centre-of-mass energy $\sqrt{s} = 300 \text{ GeV}$. Further details of this analysis can be found in [14]. Data were analysed where the FPS was in a stable position close to the circulating beam and all relevant components of the H1 detector were fully operational. The corresponding integrated luminosity amounts to 3.3 pb^{-1} . In order to study the reaction $\gamma p \rightarrow Xp'$, events were selected with a reconstructed track in the FPS, a positron candidate in one of the small-angle electron detectors of the luminosity system and at least one reconstructed track in the central H1 detector. At the trigger level, a signal in each of the components was required. Events with energy deposition in the photon detector of the luminosity system were rejected, since this indicates the presence of an event from the Bethe-Heitler process in the same bunch crossing or initial or final state radiation.

At least one track in the H1 detector was required to have a transverse momentum above 0.5 GeV and a polar angle θ in the range of $20^\circ < \theta < 160^\circ$ in order to guarantee a good trigger and reconstruction efficiency. In order to reject background from interactions of the beam with the residual gas in the beam pipe, the z coordinate of the event vertex was restricted to $|z_{\text{Vtx}}| < 35 \text{ cm}$. Further background rejection conditions were imposed, which require the timing of the event to match the bunch crossing time.

The scattered proton energy range was restricted to $540 \text{ GeV} < E'_p < 740 \text{ GeV}$ and the proton transverse momentum range to $0 < p_T \leq 0.2 \text{ GeV}$, where the FPS acceptance is well understood. The data were grouped into five 40 GeV wide intervals in E'_p . The scattered electron energies were measured in two calorimeters allowing the data to be divided into three ranges of W . The average values of W in each of these ranges were 91 GeV , 187 GeV and 231 GeV . This W range together with the measured z range corresponds to values of M_X between 32 GeV and 130 GeV , assuming the scattering is elastic at the proton vertex. The total number of events selected was 23072.

2.3 Cross Section Measurement

To obtain the differential cross section $d^3\sigma_{ep \rightarrow e'Xp'}/dydQ^2dz$, where $y = W^2/s$ and where the scattered proton p_T is integrated over the range $0 < p_T < 0.2 \text{ GeV}$, the data are corrected for acceptances and efficiencies. The PHOJET [15] Monte Carlo programme, a general photoproduction model, was used to correct for central track reconstruction efficiencies. The acceptance of the FPS was studied using both PHOJET and POMPYT [16], which is a Monte Carlo model

for diffractive hard scattering, also capable of describing reactions mediated by pion exchange. Corrections are made for the FPS trigger efficiency, the FPS track reconstruction efficiency, the track multiplicity dependent trigger efficiency of the central tracker and the electron tagger acceptances. The latter includes a correction for cases where events are lost due to an energy deposition in the photon detector by an overlaid Bethe-Heitler event. Bin by bin factors are used to correct for track reconstruction inefficiency in the H1 tracking chambers, to compensate for the migrations between proton energy intervals and to take the limited FPS acceptance into account. The values for the migration corrections vary between 0.91 and 1.13 for the intervals defined in section 3.1. The correction factor for the fraction of events lying outside the FPS acceptance region ranges between 0.27 to 0.90 with an average value of about 0.70.

The differential cross section $d\sigma_{\gamma p \rightarrow X p'}(W, z)/dz$ is determined using the relation

$$\frac{d^3\sigma_{ep \rightarrow eXp'}(W, Q^2, z)}{dydQ^2dz} = \mathcal{F}_{\gamma/e}(y, Q^2) \frac{d\sigma_{\gamma p \rightarrow X p'}(W, z)}{dz}, \quad (1)$$

where $\mathcal{F}_{\gamma/e}(y, Q^2)$ is the photon flux in the Equivalent Photon Approximation [17]. The effects of initial and final state radiation from the electron are suppressed in this analysis by the veto of events with energy deposition in the small angle photon detector. Radiative corrections are thus expected to be small [18] and have been neglected throughout the analysis.

The measured cross sections are defined solely in terms of the specified ranges in the scattered proton transverse momentum, W and z . No subtractions have been made for the contribution of protons from the decay of baryon resonances or proton dissociation processes. The major source, the $\Delta(1232)$, has been estimated to contribute at the 10% level to the total cross section for leading proton production in the range $0.6 < z < 0.9$ in DIS [19], concentrated at low z . Assuming a contribution of similar magnitude in photoproduction, this will be suppressed to the percent level by the restriction of this measurement to proton transverse momenta $p_T < 0.2$ GeV and $z > 0.66$.

2.4 Background

The following sources of background were studied:

- Protons in the FPS originating from interactions of the proton beam with the beam pipe wall or residual gas: the background actually entering the sample where a trajectory is indistinguishable from that of a proton which was scattered in an ep process at the interaction point has been found to be much less than 1% from studies of non-interacting proton bunches. This background has been neglected.
- Tracks in the central H1 detector produced by beam gas interactions: this background has been estimated using the distribution of z_{Vtx} . This is approximately distributed as a Gaussian around a mean value close to the nominal interaction point for ep interactions while beam gas interactions have a more uniform distribution in z_{Vtx} . The fraction of background events entering the data sample, where $|z_{Vtx}| < 35$ cm is required, can be estimated from the tails of the z_{Vtx} distribution and has been determined to vary between 2.2% (lowest y interval) and 3.4% (highest y interval). This has been subtracted.

- Bethe-Heitler events $ep \rightarrow e'p'\gamma$: these are not a significant source of background unless they overlap with a photoproduction event. The acceptance of the photon detector of the luminosity system for the photons is large. With the cut imposed on the maximum energy deposited in the photon detector, this background has been suppressed to the level of 0.25%, determined statistically from the probability of random overlap. This has been subtracted.

2.5 Systematic errors

The systematic uncertainties in the measurement can be grouped into those depending on y , those related to the proton energy (or z) interval and normalisation errors.

Errors depending on y . The following sources contribute to this type of error: errors on the acceptance of the electron taggers; errors on the selection efficiency for tracks in the H1 tracking chambers; migration uncertainties between adjacent y intervals and errors on the proton beam induced background in the central region of the H1 detector. The resulting uncertainties were found to vary between 6.5 and 8.5%.

Errors depending on z . The largest uncertainty arises from the acceptance correction for migrations about the measurement limit at the proton transverse momentum of $p_T = 0.2$ GeV. The uncertainty was evaluated using the PHOJET and POMPYT Monte Carlo generators. Uncertainties in the FPS calibration constants lead to systematic errors on the migration corrections between proton energy bins. This effect has also been studied using the PHOJET and POMPYT Monte Carlo models. The z dependent errors were found to vary between 2.6 and 14.1%.

Normalisation errors. These are dominated by overall FPS uncertainties such as alignment errors and uncertainties on the hodoscope efficiencies. The uncertainty in the luminosity measurement, in the vertex cut efficiency and in the positron beam related background are also included. This error amounts to 5.3%.

3 Results

3.1 The differential cross section $d\sigma_{\gamma p \rightarrow X p'}(W, z)/dz$

The cross section $d\sigma_{\gamma p \rightarrow X p'}(W, z)/dz$ for $W = 91, 187$ and 231 GeV and five values of z in the range $0.68 \leq z \leq 0.88$ is shown in figure 2. The values are listed in Table 1. It is observed that for all z and W , the measured cross sections are compatible with each other within the experimental errors. The data may be represented by a single average cross section value of $d\sigma(W, z)/dz = (8.05 \pm 0.06 \text{ (stat)} \pm 0.89 \text{ (syst)}) \mu\text{b}$. The restriction in the transverse momentum of the final state proton to $p_T \leq 0.2$ GeV implies that the measured cross section represents $(23 \pm 2 \text{ (stat)} \pm 5 \text{ (syst)})\%$ of the full differential cross section $d\sigma/dz$ in photoproduction if

the t dependence is assumed to follow e^{bt} with $b = (6.6 \pm 0.7 \text{ (stat)} \pm 1.5 \text{ (syst)}) \text{ GeV}^{-2}$ (see section 3.2). The ratio of photoproduction events with a leading proton of $0.66 \leq z \leq 0.90$ and $p_T < 0.2 \text{ GeV}$ to all photoproduction events [18] is $(1.17 \pm 0.02 \text{ (stat)} \pm 0.15 \text{ (syst)})\%$.

From the observation that the cross section $d\sigma/dz$ is independent of z and W within errors, we infer that $d\sigma/dM_X^2$ is also approximately independent of M_X at fixed W . This observation is different from pomeron exchange processes, dominant at lower M_X/W , where a $d\sigma/dM_X^2 \sim 1/M_X^2$ dependence is a good approximation to the data [4]. The present measurement is reminiscent of data from proton-proton scattering $pp \rightarrow Xp'$ at lower centre-of-mass energies squared $s < 3900 \text{ GeV}^2$ [1, 20], where a flattening of the cross section $d\sigma/dM_X^2$ is observed for masses above $M_X/\sqrt{s} \sim 0.2$.

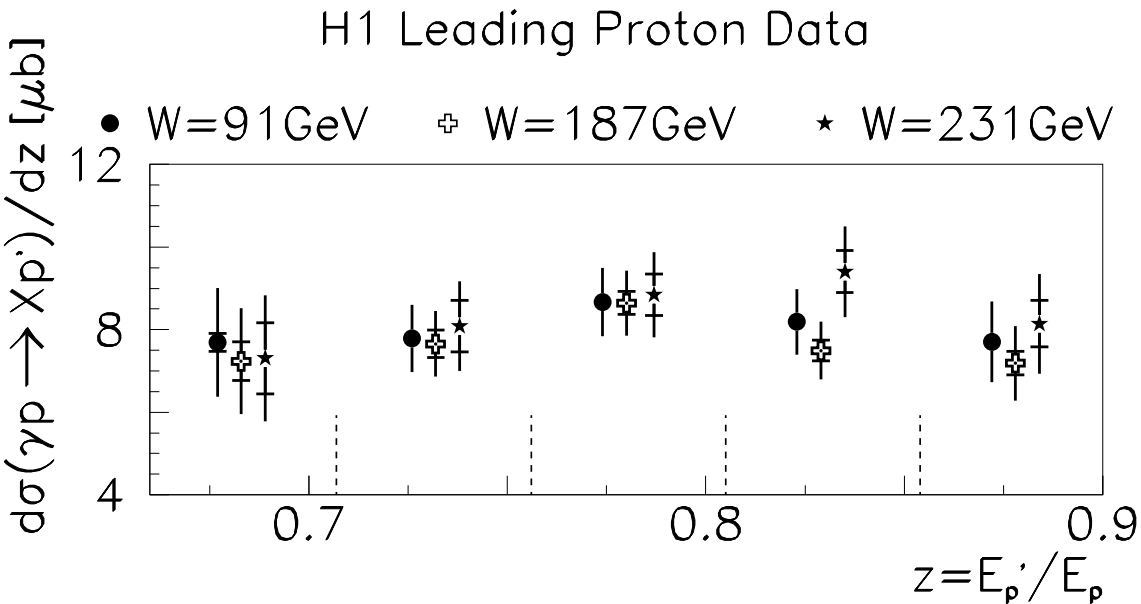


Figure 2: The cross section $d\sigma_{\gamma p \rightarrow Xp'}/dz$ as a function of z for three values of W . The inner error bar is the statistical and the outer is the total error (statistical and systematic error added in quadrature). The dashed lines show the limits of the z intervals from which the differential cross sections are obtained. The data points for $W = 91$ and $W = 231 \text{ GeV}$ are displaced in z for visibility.

In section 3.2, the measured cross-section $d\sigma/dz$ is interpreted in a Regge motivated model. The lack of W dependence of the cross section is also supportive of the hypothesis of limiting fragmentation [21] which states that target fragmentation is independent of projectile energy and type.

3.2 Triple Regge Analysis

In the language of Regge phenomenology, the W and z dependences of $d\sigma/dz$ yield information about the exchange mechanisms contributing to leading proton photoproduction. A framework

to model the process $\gamma p \rightarrow X p'$ is offered by ‘‘Triple Regge’’ phenomenology using the Mueller-Regge approach² [22], as illustrated in figure 3. The total cross section at fixed M_X is obtained from a coherent sum of the amplitudes for the exchange of Regge trajectories α_i , figure 3a, which is related, through the generalised optical theorem [22], to the forward amplitude (figure 3b) for the process $\gamma \alpha_i(t) \rightarrow \gamma \alpha_i(t)$ at an effective centre of mass energy M_X . If M_X^2 is much larger than the hadronic mass scale s_0 and $W^2 \gg M_X^2$, this forward amplitude can be expressed as a further sum of Regge trajectories α_k as shown in figure 3c. Here we neglect the possibility of interference contributions, such that the two Regge trajectories coupling to the proton in the Triple Regge diagram of figure 3c are always identical. The cross section can then be expressed as a sum over the contributing Regge trajectories [23]

$$\frac{d^2\sigma}{dt dz} = W^2 \frac{d^2\sigma}{dt dM_X^2} = \frac{s_0}{W^2} \sum_{i,k} G_{iik}^{\gamma p \rightarrow X p}(t) \left(\frac{W^2}{M_X^2} \right)^{2\alpha_i(t)} \left(\frac{M_X^2}{s_0} \right)^{\alpha_k(0)}, \quad (2)$$

where α_i refers to the trajectory exchanged between the photon and the proton and α_k refers to the additional trajectory describing the total cross section between α_i and the photon. The product of the couplings of trajectory i to the proton, trajectory k to the photon and the three-Reggeon (iik) coupling is represented by $G_{iik}^{\gamma p \rightarrow X p}(t)$.

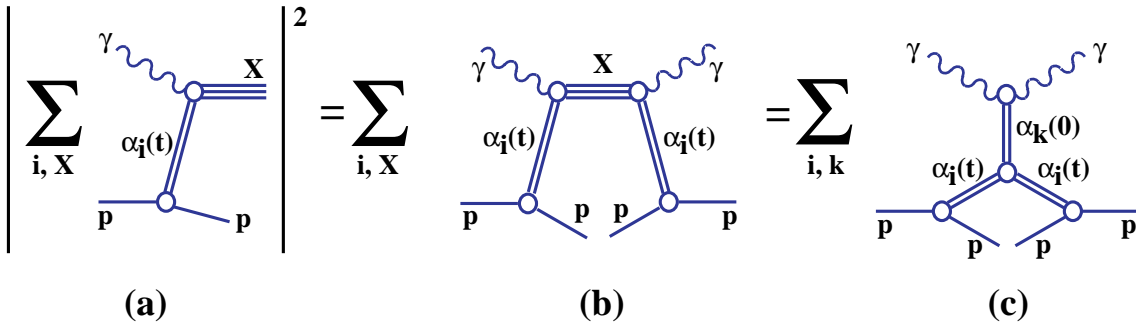


Figure 3: Illustration of the Mueller-Regge model for the inclusive photon dissociation cross section.

In [4], Triple Regge fits to lower M_X photoproduction data showed dominant pomeron exchange at the largest z and W , with further trajectories consistent with \mathbb{IR} contributing at smaller W or z . At the larger M_X/W values of the present study, the full mixture of contributing trajectories and their interferences is presumably rather complicated. The data are not sufficiently precise and do not cover a wide enough kinematic region to make a full decomposition. Instead we consider single effective trajectories α_i and α_k and assume that these represent averages of the mixtures contributing to the reaction. It is further assumed that all t dependent terms can be absorbed into a single exponential e^{bt} , where $b = b_0 - 2\alpha'_i \ln(1-z)$. The z dependent term in this expression arises from the t dependence of the trajectory of the form $\alpha_i(t) = \alpha_i(0) + \alpha'_i t$.

²This approach is normally recommended for the kinematic range $1-z = M_X^2/W^2 \ll 1$. However, since the exact region of applicability is uncertain, the approach has been applied here to test the validity of the model and to investigate the contributing exchanges.

With these assumptions, after integration over t , equation 2 becomes

$$\frac{d\sigma}{dz} = W^2 \frac{d\sigma}{dM_X^2} = \frac{A}{b} s_0^{1-\alpha_k(0)} (e^{bt_{min}} - e^{bt_{max}}) (W^2)^{2\alpha_i(0)-1} (M_X^2)^{\alpha_k(0)-2\alpha_i(0)} \quad (3)$$

where $|t_{min}|$ is the minimum kinematically allowed value of $|t|$, $|t_{max}|$ is the maximum value allowed by the experimental limit of $p_T \leq 0.2 \text{ GeV}$ for the leading proton, A is an overall normalisation factor and s_0 is taken to be 1 GeV^2 following the usual convention [1].

The observed approximate independence of $d\sigma/dz$ of M_X^2 and W implies in equation 3 that $2\alpha_i(0) - 1 \sim 0$ and $\alpha_k(0) - 2\alpha_i(0) \sim 0$, i.e. $\alpha_i(0) \sim 0.5$ and $\alpha_k(0) \sim 1$. A fit of the full ansatz of equation 3 to the data with A , b_0 , $\alpha_i(0)$ and $\alpha_k(0)$ as free parameters, taking α'_i to be $(1.0 \pm 0.2) \text{ GeV}^{-2}$ [1, 24], gives

$$\begin{aligned} \alpha_i(0) &= 0.33 \pm 0.04 \text{ (stat)} \pm 0.04 \text{ (syst)}, \\ \alpha_k(0) &= 0.99 \pm 0.01 \text{ (stat)} \pm 0.05 \text{ (syst)}, \\ b_0 &= (3.6 \pm 0.7 \text{ (stat)} \pm 1.4 \text{ (syst)}) \text{ GeV}^{-2} \text{ and} \\ A &= (495 \pm 92 \text{ (stat)} \pm 320 \text{ (syst)}) \mu\text{b}/\text{GeV}^2. \end{aligned}$$

In each case, the first error quoted is the statistical and the second is the systematic uncertainty, which includes a contribution from the variation³ of α'_i . The fit gives a good representation of the data within the dominant systematic errors. This is illustrated in figures 4a-e which show the values of $d\sigma/dz$ as a function of W in each z bin with the fit, represented by the solid curves, superimposed.

For the mean value in the data of $z = 0.78$, the value of b_0 extracted from the fit implies that $b = (6.6 \pm 0.7 \text{ (stat)} \pm 1.5 \text{ (syst)}) \text{ GeV}^{-2}$. The value of b determined in this indirect manner is compatible within experimental errors with that found by direct measurement by ZEUS [25] for $p_T^2 < 0.5 \text{ GeV}^2$. The values of $\alpha(0)$ for the π , \mathcal{IR} and Pomeron trajectories are approximately 0, 0.5 and 1.0, respectively [1]. Hence, within the framework of the applied model, we deduce from the extracted value of $\alpha_i(0)$ that the exchange between the photon and the proton can be understood as a mixture of trajectories, dominated by π and \mathcal{IR} , consistent with the previous H1 measurement at higher Q^2 [3]. In addition since $\alpha_k(0)$ is close to unity, the total cross section for the scattering between the mixture of Regge trajectories represented by α_i and the photon seems to be dominated by pomeron exchange, as would be expected for total cross sections at these energies ($32 \text{ GeV} < M_X < 130 \text{ GeV}$).

Inclusive proton reactions $pp \rightarrow Xp'$ have been studied extensively in the framework of Triple Regge models [26–28]. The present measurements are compared with $pp \rightarrow Xp'$ data using the fits described in [28]. Vertex factorisation is assumed, such that the ratio of couplings in the γp and pp cases is given by

$$\left[\frac{G_{ii\mathcal{IR}}^{\gamma p \rightarrow Xp}(t)}{G_{ii\mathcal{IR}}^{pp \rightarrow Xp}(t)} \right] = \left[\frac{\sigma_{tot}^{\gamma p}}{\sigma_{tot}^{pp}} \right]_{s \rightarrow \infty} = 0.0031, \quad (4)$$

³Setting α'_i to zero, the fit gives the almost identical values of $\alpha_i(0) = 0.35$ and $\alpha_k(0) = 0.99$ with similar errors.

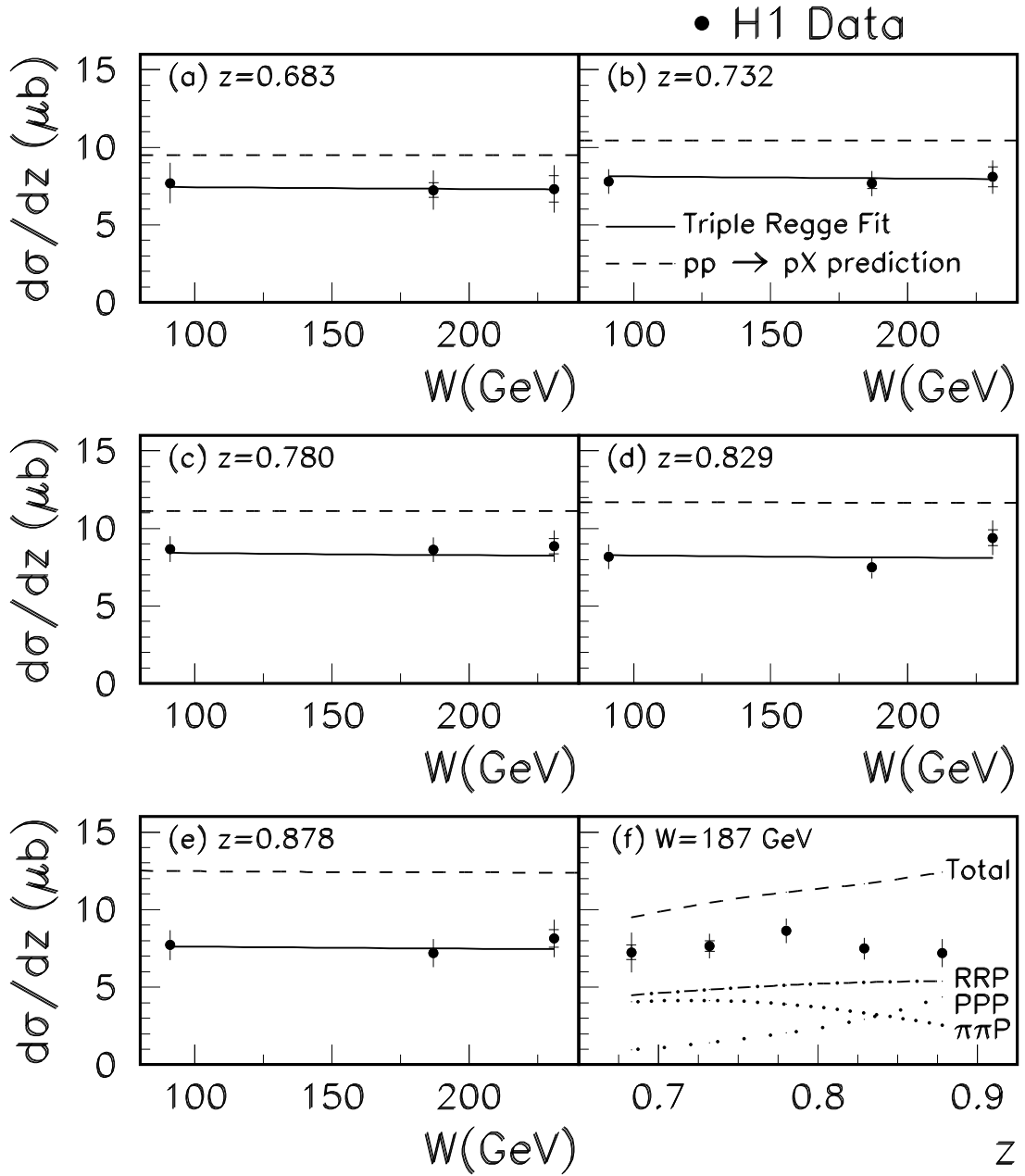


Figure 4: (a-e) The differential cross sections $d\sigma/dz$ as a function of W for each measured z value. The data are compared with the result of the Triple Regge fit described in the text (solid curves) and with the prediction derived from Triple Regge analysis of $pp \rightarrow Xp'$ data [28] (dashed curves). (f) The measured cross section as a function of z at $W = 187$ GeV, compared with the prediction derived from Triple Regge analysis of $pp \rightarrow Xp'$ data [28]. The decomposition into the three dominant terms is also shown.

where s is the square of the centre of mass energy and the numerical value of 0.0031 for the ratio of total cross sections is taken from [29]. Equation 2 is then used to obtain the W and z dependences of the cross section for $\gamma p \rightarrow Xp'$ assuming the couplings and Regge trajectories given in [28].⁴ In this model, the dominant contributions for the present kinematic range are $\pi\pi\mathcal{I}\mathcal{P}$, $\mathcal{I}\mathcal{R}\mathcal{I}\mathcal{P}$ and $\mathcal{I}\mathcal{P}\mathcal{I}\mathcal{P}$, all other terms being negligible. The total predicted cross section is shown in figures 4a-e (dashed curves). The prediction at $W = 187$ GeV and its decomposition into the three dominant Triple Regge terms are shown in figure 4f.

The predicted photoproduction cross sections lie 25 – 65% above the measured values (see figure 4), which can be considered as fair agreement given the simplicity of the model and the uncertainties. Hence $pp \rightarrow Xp'$ and $\gamma p \rightarrow Xp'$ data away from the pomeron exchange dominated region can be reasonably well described within a single relatively simple Triple Regge model. This contrasts with the discrepancies of an order of magnitude or more observed when predicting diffractive hard scattering cross sections at larger z in $\bar{p}p$ collisions at the Tevatron [30] using parton densities extracted from diffractive DIS at HERA [6, 7].

3.3 Leading Proton Production in DIS and Photoproduction

In this section, the photoproduction cross sections with a leading proton are combined with data from deep inelastic scattering with a leading proton in the range $0.71 < z < 0.90$, published in [3]. Since the DIS and photoproduction leading proton data were recorded under very similar experimental conditions, the bulk of the systematic errors are identical and thus have little impact on the analysis. Comparing the photoproduction and DIS data allows one to study changes in the scattering process as the incoming projectile changes from a hadron-like object at $Q^2 = 0$ to a point-like probe at higher Q^2 . The DIS data sample covered the range $2 \text{ GeV}^2 \leq Q^2 \leq 50 \text{ GeV}^2$ and $6 \cdot 10^{-5} \leq x \leq 6 \cdot 10^{-3}$, where x is the Bjorken scaling variable. A leading proton structure function $F_2^{LP(3)}$ was defined as:

$$\frac{d^3\sigma}{xdQ^2dz} = \frac{4\pi\alpha^2}{xQ^4} \left(1 - y + \frac{y^2}{2[1 + R(x, Q^2, z)]} \right) F_2^{LP(3)}(x, Q^2, z), \quad (5)$$

where α denotes the electromagnetic coupling constant, y the inelasticity variable and $R(x, Q^2, z)$ the ratio of the longitudinal to the transverse polarised photon induced DIS cross sections with a leading proton. Due to the y^2 factor, the impact of $R(x, Q^2, z)$ on the measurement of the structure function $F_2^{LP(3)}(x, Q^2, z)$ is small and R was set to zero in [3]. The structure function $F_2^{LP(3)}$ is related to the $\gamma^* p$ cross section by

$$\frac{d\sigma_{\gamma^{(*)}p \rightarrow Xp'}(Q^2, W, z)}{dz} = \frac{4\pi^2\alpha}{Q^2} F_2^{LP(3)}(x, Q^2, z). \quad (6)$$

The DIS cross sections $d\sigma/dz$ deduced from the values of $F_2^{LP(3)}$ using equation 6, are shown together with the photoproduction measurement reported here in figure 5 for the data in

⁴The couplings in table 3 of [28] from the fit with the restriction $G_{\pi\pi\mathcal{I}\mathcal{P}}^{pp \rightarrow Xp} < 300 \text{ mb GeV}^{-2}$ are used. The trajectories are $\alpha_{\mathcal{I}\mathcal{P}}(t) = 1 + 0.25t$, $\alpha_{\mathcal{I}\mathcal{R}}(t) = 0.5 + t$ and $\alpha_{\pi}(t) = t$. The t dependence of each Triple Regge coupling is parameterised with a single exponential.

the range $40 \text{ GeV} < M_X < 60 \text{ GeV}$ at $z = 0.732, 0.780, 0.829$ and 0.878 . The data at other values of M_X (not shown) have a very similar Q^2 dependence. For all values of z investigated, the data approach $Q^2 = 0 \text{ GeV}^2$ in a qualitatively similar manner to that observed for the inclusive ep cross section [9, 10].

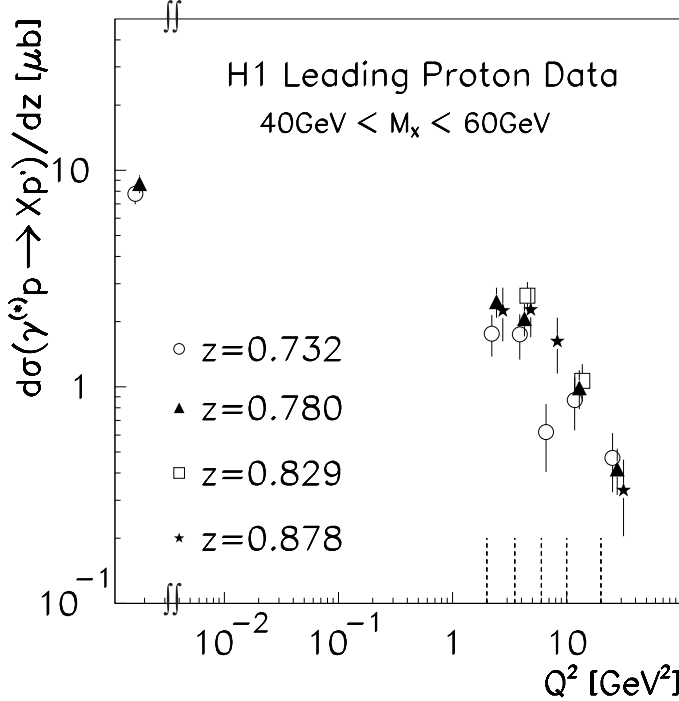


Figure 5: The cross section $d\sigma_{\gamma^{(*)}p \rightarrow Xp'}/dz$ as a function of Q^2 for four values of z in the interval $40 \text{ GeV} < M_X < 60 \text{ GeV}$. The DIS data points are derived from [3]. The data points in the same Q^2 bin are displaced in Q^2 for visibility. The dashed lines indicate the bin limits in Q^2 .

A more sensitive quantity with which to study the transition from DIS to photoproduction is the ratio of the semi-inclusive to inclusive cross sections. For photoproduction, the ratio f_{LP} of leading proton production per unit z to the total cross section is defined as

$$f_{LP}(Q^2 \approx 0, W, z) = \frac{d\sigma_{\gamma p \rightarrow Xp'}/dz(Q^2 \approx 0, W, z)}{\sigma_{tot}^{\gamma p}(W)}, \quad (7)$$

where $\sigma_{tot}^{\gamma p}$ was taken from the Donnachie and Landshoff parametrisation in [29] of the form

$$\sigma_{tot}^{\gamma p} = 68 \left(\frac{W^2}{\text{GeV}^2} \right)^{0.0808} + 129 \left(\frac{W^2}{\text{GeV}^2} \right)^{-0.4525} \mu\text{b}. \quad (8)$$

For DIS, the ratio of leading proton production per unit z to the inclusive process is obtained from

$$f_{LP}(Q^2, W, z) = \frac{F_2^{LP(3)}(x, Q^2, z)}{F_2^{\text{H1QCD}}(x, Q^2)}, \quad (9)$$

where $F_2^{\text{H1QCD}}(x, Q^2)$ is a parametrisation of the proton structure function taken from a QCD fit to the data in [31]. Note that $W \approx \sqrt{Q^2/x}$ at low x .

The ratios $f_{\text{LP}}(Q^2, W, z)$ are shown in figure 6, separately for each z value in four ranges of W . The fraction of leading proton events in the z range under study is found to increase⁵ with Q^2 from $\sim 5\%$ per unit z in photoproduction ($Q^2 \sim 0 \text{ GeV}^2$) to about 10% per unit z at $Q^2 \sim 10 \text{ GeV}^2$ at all z and W .

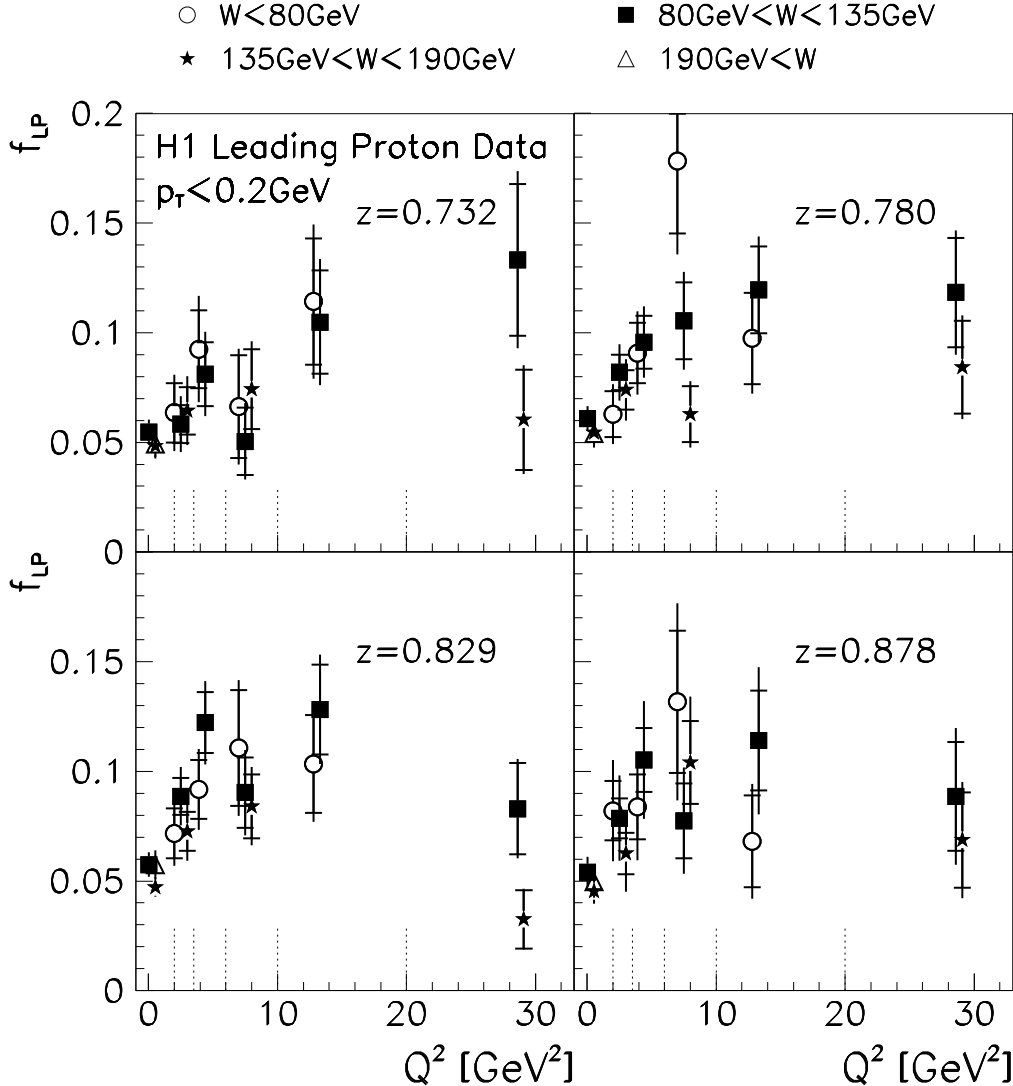


Figure 6: The ratio per unit z , f_{LP} , of the number of leading proton events for four values of z to the total in four intervals of W as a function of Q^2 . The data points in the same Q^2 bin are displaced in Q^2 for visibility. The dashed lines indicate the bin limits in Q^2 .

The observed rise of f_{LP} from low to high Q^2 in figure 6 cannot fully be explained by

⁵ The χ^2 for the DIS data in figure 6 to be compatible with the mean values of the photoproduction data is computed for each z value. The result is a total χ^2 of 141 for 48 degrees of freedom, evaluated using the full experimental errors.

any reasonable Q^2 dependence of the t slope and thus indicates a breaking of factorisation of the proton from the photon vertex. A similar suppression of the cross section relative to predictions based on vertex factorisation has been observed in diffractive dijet production in regions where the photon is resolved [32] and in the process $pp \rightarrow Xp$ at high energy [2]. Absorptive corrections, corresponding to multiple Reggeon exchange, would be expected to give rise to such an effect [33]. It could also be due to the onset with increasing Q^2 of the cross section for longitudinally polarised photons if the relative contribution of the longitudinal cross section is different in the semi-inclusive and inclusive cases.

4 Summary

Photoproduction reactions with a final state proton of $p_T \leq 0.2$ GeV observed in the H1 Forward Proton Spectrometer (FPS) have been analysed in the kinematic range $0.66 \leq z \leq 0.90$ at γp centre-of-mass energies $W = 91, 187$ and 231 GeV. The cross section $d\sigma(W, z)_{\gamma p \rightarrow Xp'}/dz$ was determined to be on average 8.05 ± 0.06 (stat) ± 0.89 (syst) μb , independent of z and W within the experimental errors.

A fit of a Triple Regge model to the data gives a good representation. In this model, the proton-photon interaction can be described by the exchange of an effective trajectory having $\alpha_i(0) = 0.33 \pm 0.04$ (stat) ± 0.04 (syst), consistent with a mixture of pions and members of the exchange degenerate trajectory \mathcal{IR} with $\alpha_{\mathcal{IR}}(0) \sim 0.5$. This result is consistent with the findings at similar z in deep inelastic scattering. The total cross section for the interaction of the mixture of trajectories α_i with the photon is described by $\alpha_k(0) = 0.99 \pm 0.01$ (stat) ± 0.05 (syst), implying that it is dominated by the pomeron term. The exponential slope parameter describing the t dependence of the data is indirectly determined within this model to be $b = (6.6 \pm 0.7$ (stat) ± 1.5 (syst)) GeV^{-2} at $z = 0.78$. A more detailed Triple Regge model of $pp \rightarrow Xp$ data [28] has been extended to describe dissociative photoproduction by assuming vertex factorisation and gives a reasonable description of the measurements.

The data from photoproduction and deep inelastic scattering with a final state proton observed in the FPS show a qualitatively similar Q^2 dependence to that observed when going from virtual to real photons in the inclusive reaction $\gamma^{(*)}p \rightarrow X$. The cross section for leading proton production expressed as a fraction per unit z of the total $\gamma^{(*)}p$ cross section, has been studied as a function of Q^2 in intervals of z and W . This fraction has been found to increase with Q^2 .

Acknowledgements

We are grateful to the HERA machine group whose outstanding efforts have made and continue to make this experiment possible. We thank the engineers and technicians for their work in constructing and now maintaining the H1 detector, our funding agencies for financial support, the DESY technical staff for continual assistance and the DESY directorate for the hospitality which they extend to the non DESY members of the collaboration. The forward proton spectrometer was supported by the INTAS93-43 project and the NATO contract PST.CLG.975100.

References

- [1] K. Goulianos, Phys. Rept. **101** (1983) 169 and references therein.
- [2] N. Amos *et al.* [E710 Collaboration], Phys. Lett. B **301** (1993) 313;
F. Abe *et al.* [CDF Collaboration], Phys. Rev. D **50** (1994) 5535.
- [3] C. Adloff *et al.* [H1 Collaboration], Eur. Phys. J. C **6** (1999) 587 [hep-ex/9811013].
- [4] C. Adloff *et al.* [H1 Collaboration], Z. Phys. C **74** (1997) 221 [hep-ex/9702003].
- [5] J. Breitweg *et al.* [ZEUS Collaboration], Z. Phys. C **75** (1997) 421 [hep-ex/9704008].
- [6] C. Adloff *et al.* [H1 Collaboration], Z. Phys. C **76** (1997) 613 [hep-ex/9708016].
- [7] J. Breitweg *et al.* [ZEUS Collaboration], Eur. Phys. J. C **6** (1999) 43 [hep-ex/9807010].
- [8] J. Breitweg *et al.* [ZEUS Collaboration], Eur. Phys. J. C **1** (1998) 81 [hep-ex/9709021].
- [9] C. Adloff *et al.* [H1 Collaboration], Nucl. Phys. B **497** (1997) 3 [hep-ex/9703012].
- [10] J. Breitweg *et al.* [ZEUS Collaboration], Phys. Lett. B **487** (2000) 53 [hep-ex/0005018].
- [11] I. Abt *et al.* [H1 Collaboration], Nucl. Instrum. Meth. A **386** (1997) 310.
- [12] P. Van Esch *et al.*, Nucl. Instrum. Meth. A **446** (2000) 409 [hep-ex/0001046].
- [13] B. List, DESY-F11-F22-97-03, see http://www-h1.desy.de/publications/theses_list.html.
- [14] H. Mahlke-Krüger, DESY-THESIS-2000-004,
see http://www-h1.desy.de/publications/theses_list.html;
C. Wittek, DESY-THESIS-1998-002,
see http://www-h1.desy.de/publications/theses_list.html.
- [15] R. Engel, “PHOJET manual (Program version 1.05c, June 96)”, University of Siegen preprint 95-05 (1995) (revised Feb. 96);
R. Engel and J. Ranft, Phys. Rev. D **54** (1996) 4244 [hep-ph/9509373].
- [16] P. Bruni, A. Edin, G. Ingelman, “POMPYT version 2.6 – A Monte Carlo Program to Simulate Diffractive Hard Scattering Processes”, unpublished program manual (1996), see <http://www3.tsl.uu.se/theppompyt>;
P. Bruni and G. Ingelman, DESY-93-187 *Presented at Europhysics Conference on High Energy Physics, Marseille, France, 22-28 Jul 1993*.
- [17] S. Frixione, M.L. Mangano, P. Nason and G. Ridolfi, Phys. Lett. B **319** (1993) 339 [hep-ph/9310350].
- [18] S. Aid *et al.* [H1 Collaboration], Z. Phys. C **69** (1995) 27 [hep-ex/9509001].
- [19] A. Szczurek, N. N. Nikolaev and J. Speth, Phys. Lett. B **428** (1998) 383 [hep-ph/9712261].
- [20] M.G. Albrow *et al.*, Nucl. Phys. B **108** (1967) 1.

- [21] J. Benecke, T. T. Chou, C. N. Yang and E. Yen, Phys. Rev. **188** (1969) 2159;
T. T. Chou and C. N. Yang, Phys. Rev. D **50** (1994) 590.
- [22] A. H. Mueller, Phys. Rev. D **2** (1970) 2963.
- [23] A. B. Kaidalov, Phys. Rept. **50** (1979) 157;
G. Alberi and G. Goggi, Phys. Rept. **74** (1981) 1;
N. Zotov and V. Tsarev, Sov. Phys. Usp. **31** (1988) 119.
- [24] W. D. Apel *et al.* [Serpukhov-CERN Collaboration], Nucl. Phys. B **154** (1979) 189 [Yad. Fiz. **30** (1979) 373].
- [25] W. Schmidke, “Leading Baryon Production in ep Scattering at HERA”, p. 924 in A. Astbury *et al.*, “High energy physics” Proceedings, 29th International Conference, ICHEP’98, Vancouver, Canada, July 23-29, 1998. Vol. 1, 2 *Singapore: World Scientific (1999) p1833*.
- [26] D. P. Roy and R. G. Roberts, Nucl. Phys. B **77** (1974) 240.
- [27] R. D. Field and G. C. Fox, Nucl. Phys. B **80** (1974) 367.
- [28] S.N. Ganguli and D. P. Roy, Phys. Rept. **67** (1980) 201.
- [29] A. Donnachie and P. V. Landshoff, Phys. Lett. B **296** (1992) 227 [hep-ph/9209205].
- [30] L. Alvero, J. C. Collins, J. Terron and J. J. Whitmore, Phys. Rev. D **59** (1999) 074022 [hep-ph/9805268];
L. Alvero, J. C. Collins and J. J. Whitmore, hep-ph/9806340;
B. E. Cox, J. R. Forshaw and L. Lönnblad, hep-ph/0012310;
T. Affolder *et al.* [CDF Collaboration], Phys. Rev. Lett. **84** (2000) 5043;
C. Royon, L. Schoeffel, J. Bartels, H. Jung and R. Peschanski, Phys. Rev. D **63** (2001) 074004 [hep-ph/0010015].
- [31] C. Adloff *et al.* [H1 Collaboration], Eur. Phys. J. C **13** (2000) 609 [hep-ex/9908059].
- [32] C. Adloff *et al.* [H1 Collaboration], Eur. Phys. J. C **6** (1999) 421 [hep-ex/9808013].
- [33] N. N. Nikolaev, J. Speth and B. G. Zakharov, [hep-ph/9708290].

z	$\langle W_{\gamma p} \rangle$ [GeV]	$d\sigma/dz$ [μb]	\pm stat \pm fps \pm wbin \pm norm	(\pm total)
0.683	91	7.69	$\pm 0.22 \pm 1.09 \pm 0.58 \pm 0.41$	($\pm 17.1\%$)
	187	7.24	$\pm 0.47 \pm 1.02 \pm 0.47 \pm 0.38$	($\pm 17.7\%$)
	231	7.31	$\pm 0.86 \pm 1.03 \pm 0.62 \pm 0.39$	($\pm 20.9\%$)
0.732	91	7.79	$\pm 0.16 \pm 0.34 \pm 0.59 \pm 0.41$	($\pm 10.4\%$)
	187	7.66	$\pm 0.33 \pm 0.33 \pm 0.50 \pm 0.41$	($\pm 10.4\%$)
	231	8.09	$\pm 0.63 \pm 0.35 \pm 0.69 \pm 0.43$	($\pm 13.4\%$)
0.780	91	8.67	$\pm 0.13 \pm 0.16 \pm 0.66 \pm 0.46$	($\pm 9.5\%$)
	187	8.64	$\pm 0.28 \pm 0.15 \pm 0.56 \pm 0.46$	($\pm 9.2\%$)
	231	8.85	$\pm 0.50 \pm 0.16 \pm 0.75 \pm 0.47$	($\pm 11.6\%$)
0.829	91	8.19	$\pm 0.12 \pm 0.21 \pm 0.62 \pm 0.43$	($\pm 9.7\%$)
	187	7.49	$\pm 0.25 \pm 0.19 \pm 0.49 \pm 0.40$	($\pm 9.4\%$)
	231	9.40	$\pm 0.51 \pm 0.24 \pm 0.80 \pm 0.50$	($\pm 11.7\%$)
0.878	91	7.71	$\pm 0.14 \pm 0.65 \pm 0.59 \pm 0.41$	($\pm 12.7\%$)
	187	7.19	$\pm 0.29 \pm 0.61 \pm 0.47 \pm 0.38$	($\pm 12.6\%$)
	231	8.15	$\pm 0.56 \pm 0.69 \pm 0.69 \pm 0.43$	($\pm 14.8\%$)

Table 1: The differential cross section $d\sigma_{\gamma p \rightarrow X p'}/dz(W, z)$ in μb for proton transvere momenta $p_T < 0.2$ GeV for five intervals in z and three intervals in W in GeV. The uncertainties quoted are the contributions arising from the statistical error (stat), the uncertainty introduced by the z measurement (fps), errors depending only on the W interval (wbin), and a common normalisation uncertainty (norm). The total relative error is given in brackets.